Facile and Efficient Electrochemical Synthesis of PbTe Dendritic Structures

Gao-Ren Li,*[,†,‡] Chen-Zhong Yao,[†] Xi-Hong Lu,[†] Fu-Lin Zheng,[†] Zhan-Ping Feng,[†] Xiao-Lan Yu,[†] Cheng-Yong Su,[†] and Ye-Xiang Tong*[,†]

MOE Laboratory of Bioinorganic and Synthetic Chemistry, School of Chemistry and Chemical Engineering, Institute of Optoelectronic and Functional Composite Materials, Sun Yat-Sen University, Guangzhou 510275, China, and State Key Lab of Rare Earth Materials Chemistry and Applications, Beijing 100871, China

Received October 28, 2007. Revised Manuscript Received March 4, 2008

We report here a facile and efficient synthesis route for the preparation of symmetrical PbTe dendritic structures consisted of orderly and regular particles via electrochemical deposition without any templates. The electrochemical reactions relevant to the growth of PbTe intermetallic compounds were studied by cyclic voltammetry, and the formation mechanism of PbTe dendritic structures was investigated. The electrode potential oscillation was relevant to the formation of the PbTe dendrites. The sizes of the particles in dendritic structures were tunable from 100 to 500 nm and the shapes could be controlled to be either starlike or trigonal. These prepared PbTe dendrites were characterized by SEM, EDS, XRD, HRTEM, and SAED, respectively. The DSC analyses were conducted to study the thermal properties of the prepared PbTe dendritic structures. The high transmittance of the PbTe dendritic structures between 500 and 4000 nm were observed, and the band gap energy of the prepared PbTe was calculated about 0.272 eV.

1. Introduction

Recently, many efforts have been focused on the hierarchical assembly of 1D nanoscale building blocks into ordered superstructures or complex architectures. The hierarchical structure is an important form among the various morphologies, which is made of building units at different levels, with the higher levels having a control or precedence over the lower levels. The hierarchical assembly of nanoscale building blocks represents a significant challenge in the field of nanoscale science and is a crucial step to realize the functional nanosystems. The branched structures have large surface areas, allow for heterostructures, and can form continuous networks compared with other structures, e.g., aggregates or 1D nanostructures, and thus they can be applied in photovoltaics and multifunctional nanoelectronics.[1] In addition, the branched structures can offer fundamental scientific opportunities for investigating the influence of size and dimensionality with respect to their collective magnetic, optical, and electronic properties and would provide possibilities to investigate the novel properties and applications resulting from the spatial orientation and arrangement of the nanocrystals. Therefore, the fabrication of the dendritic structures with well-controlled morphologies may open new opportunities for wide applications of the future nanodevices. Recently, some efforts have been devoted to the shape-controlled synthesis of dendritic structures.[2] Various methods have been explored to synthesize dentritic structures, such as template method,[3] electrochemical deposition,[4] thermal vapor transport and condensation,[5] laser-assisted catalytic growth,[6] chemical vapor deposition (CVD).[7] Among them, electrochemical deposition represents a simple, quick, and economical method for the preparation of large-area dendritic structures. It also offers a high degree of freedom in altering the interplay between the crystal growth rate and the mass transport rate, which makes it an ideal method to systematically study the dendritic growth of inorganic materials.[8]

It is well-known that lead chalcogenides are very promising materials for thermoelectric applications because of their

* Corresponding author. E-mail: ligaoren@mail.sysu.edu.cn (G.-R.L.); chedhx@mail.sysu.edu.cn (Y.-X.T.).
† Sun Yat-Sen University.
‡ State Key Lab of Rare Earth Materials Chemistry and Applications.

(1) (a) Cho, S. O.; Lee, E. J.; Lee, H. M.; Kim, J. G.; Kim, Y. J. *Adv. Mater.* **2006**, *18*, 60–65. (b) Sukhanova, A.; Baranov, A. V.; Perova, T. S.; Cohen, J. H. M.; Nabiev, I. *Angew. Chem., Int. Ed.* **2006**, *45*, 2048–2052. (c) Cao, M. H.; Liu, T. F.; Gao, S.; Sun, G. B.; Wu, X. L.; Hu, C. W.; Wang, Z. L. *Angew. Chem., Int. Ed.* **2005**, *44*, 4197–4201.
(2) (a) López, C. M.; Choi, K.-S. *Langmuir* **2006**, *22*, 10625–10629. (b) Song, Y.; Yang, Y.; Medforth, C. J.; Pereira, E.; Singh, A. K.; Xu, H.; Jiang, Y.; Brinker, C. J.; Swol, F.; Shelnutt, J. A. *J. Am. Chem. Soc.* **2004**, *126*, 635–645.
(3) (a) Ding, Y.-S.; Shen, X.-F.; Gomez, S.; Luo, H.; Aindow, M.; Suib, S. L. *Adv. Funct. Mater.* **2005**, *16*, 549–555. (b) Zhong, Z.; Yin, Y.; Gates, B.; Xia, Y. *Adv. Mater.* **2000**, *12*, 206. (c) Lu, Y.; Yin, Y.; Xia, Y. *Adv. Mater.* **2001**, *13*, 271. (d) Xia, Y.; Yin, Y.; Lu, Y.; McLellan, J. *Adv. Funct. Mater.* **2003**, *13*, 507.
(4) Xiao, Z. L.; Han, C. Y.; Kwok, W. K.; Wang, H. H.; Welp, U.; Wang, J.; Crabtree, G. W. *J. Am. Chem. Soc.* **2004**, *126*, 2316.
(5) (a) Lao, J. Y.; Wen, J. G.; Ren, Z. F. *Nano Lett.* **2002**, *2*, 1287. (b) Lao, J. Y.; Huang, J. Y.; Wang, D. Z.; Ren, Z. F. *Nano Lett.* **2003**, *3*, 235.
(6) Duan, X. F.; Lieber, C. M. *Adv. Mater.* **2000**, *12*, 298.
(7) (a) Wang, Z. L. *Annu. Rev. Phys. Chem.* **2004**, *55*, 159. (b) Pan, Z. W.; Dai, Z. R.; Wang, Z. L. *Science* **2001**, *291*, 1947.
(8) Shu, S.; Husain, S.; Koros, W. J. *J. Phys. Chem. C* **2007**, *111*, 652–657.

10.1021/cm8001942 CCC: $40.75
Published on Web 04/24/2008

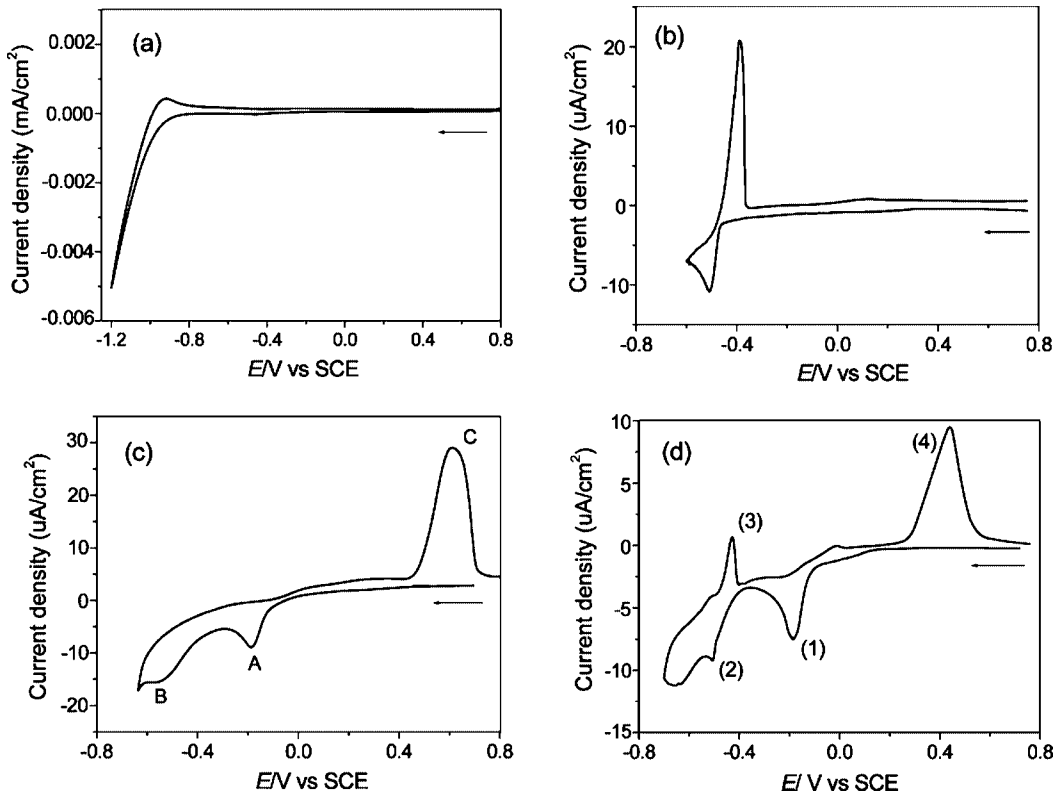

Figure 1. Cyclic voltammograms of Pt electrodes in solutions of (a) 0.1 M tartaric acid; (b) 0.005 M $Pb(NO_3)_2$ + 0.1 M tartaric acid; (c) 0.01 M Na_2TeO_3 + 0.1 M tartaric acid; and (d) 0.005 M $Pb(NO_3)_2$ + 0.01 M Na_2TeO_3 + 0.1 M tartaric acid.

narrow band gaps and rock salt structure.[9] PbTe and PbTe-based compounds are superior materials for electrical power generation devices and solid-state thermoelectric cooling.[10] Recently, much attention has been focused on enhancements in the figure of merit of PbTe by introducing nanoscopic geometrical confinement in one, two, or three dimensions or by tailoring the nanoparticle shape.[11] Therefore, the synthesis of novel PbTe structures has attracted intensive attention. In this paper, the preparation of the novel PbTe dendritic structures consisting of orderly and regular particles was first investigated via electrochemical deposition without any templates. We established a new route for controlling the shape of Pb-chalcogenide materials by controlling the electrochemical reaction kinetics with the help of an electrochemical oscillation process. This route offers a higher degree of freedom in altering the interplay between the crystal growth rate and the mass transport rate, which makes it one of the ideal methods to study the dendritic growth of inorganic materials. The electrodeposition under the help of electrochemical oscillation also represents an economical method for the preparation of large area dendritic structures. The optical properties of PbTe dendritic structures were investigated.

(9) (a) Shchennikov, V. V.; Ovsyannikov, S. V. *Solid State Commun.* **2003**, *126*, 373. (b) Zhu, J.-P.; Yu, S,-H.; He, Z.-B.; Jiang, J.; Chen, K.; Zhou, X.-Y. *Chem. Commun.* **2005**, 5802–5804.

(10) Hsu, K. F.; Loo, S.; Guo, F.; Chen, W.; Dyck, J. S.; Uher, C.; Hogan, T.; Polychroniadis, E. K.; Kanat-zidis, M. G. *Science* **2004**, *303*, 818.

(11) (a) Venkatasubramanian, R.; Siivola, E.; Colpitts, T.; Quinn, B. O. *Nature* **2001**, *413*, 597. (b) Harman, T. C. P.; Taylor, J.; Walsh, M. P.; LaForge, B. E. *Science* **2002**, *297*, 2229. (c) Shi, W.; Yu, J.; Wang, H.; Zhang, H. *J. Am. Chem. Soc.* **2006**, *128*, 16490–16491.

2. Experimental Section

The electrochemical deposition of PbTe thin films was carried out in a solution of $Pb(NO_3)_2$ and Na_2TeO_3. To control the surface shapes of PbTe films, we added tartaric acid to the deposition bath. A simple three-electrode cell was used in our experiments. A graphite electrode was used as a counter electrode (spectral grade, 1.8 cm^2). A saturated calomel electrode (SCE) was used as the reference electrode that was connected to the cell with a double salt bridge system. All potential values determined in this study were the values vs SCE. A pure Pt wire (99.99%, 0.1 cm^2) was used as working electrode during the measuring of cyclic voltammogram, and a pure Cu plate (99.99%, 1.0 cm^2) was used as working electrode during electrodeposition. The electrodeposition experiments were carried out by galvanostatic electrolysis at room temperature. The cyclic voltammogram measurements were carried out in a Chi750B electrochemical workstation. The obtained PbTe deposits were analyzed by X-ray diffraction (XRD, PIGAKU, D/MAX 2200 VPC) to determine the film structures. The surface morphologies of the as-deposited films were observed by field emission scanning electron microscopy (FE-SEM, JSM-6330F), thermal field emission environment scanning electron microscopy (TFE-SEM, FEI, Quanta 400), and transmission electron microscopy (TEM, JEM-2010HR). The thermal properties of the as-prepared PbTe dendritic structures was carried out by a differential thermal analyzer (DTA 1700, Perkin-Elmer) under a nitrogen atmosphere with the temperature increasing at a rate of 5 °C/min. Optical properties were tested with an infrared ray spectrometer (FT-IR, Nicolet 330).

3. Results and Discussion

Figure 1a shows the cyclic voltammogram (CV) of Pt electrode in a solution of 0.1 M tartaric acid as a blank CV.

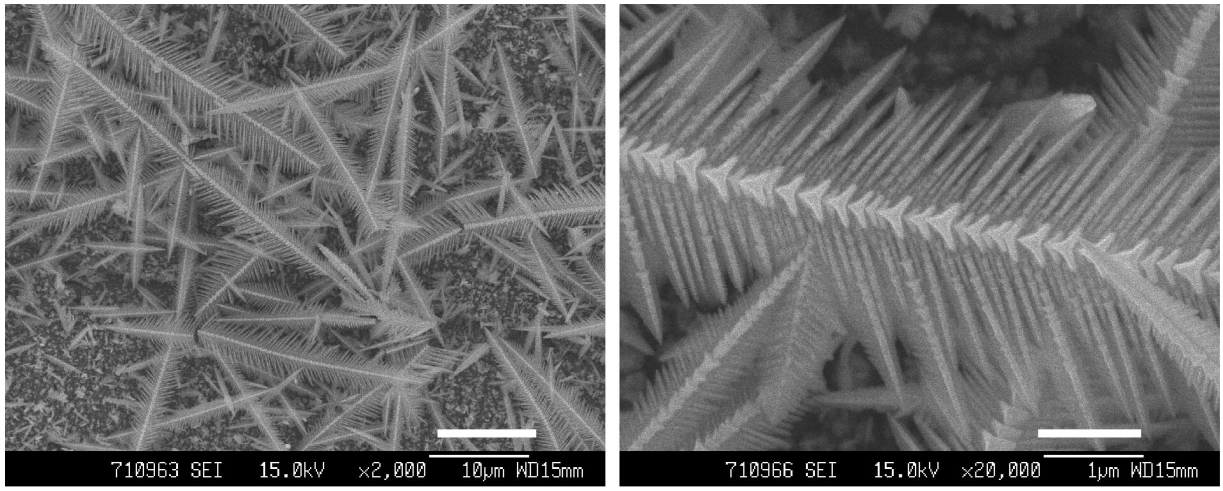

Figure 2. SEM images of PbTe dendritic structures prepared in a 0.005 M $Pb(NO_3)_2$ + 0.01 M Na_2TeO_3 + 0.10 M tartaric acid solution with a current density of 3.33 mA/cm^2 for 30 min. (a) Panorama of PbTe deposit (scan bar is 10 μm); (b) single dendrite (scan bar is 1 μm).

Figure 1b shows the CV of a Pt electrode in solution of 0.005 M $Pb(NO_3)_2$ + 0.1 M tartaric acid. One cathodic reduction wave was observed, and its peak potential appeared at about –0.51 V. This reduction wave corresponded to the reduction of Pb^{2+} to Pb. A sharp oxidation wave was also observed at about –0.39 V, which corresponded to the anodic stripping of Pb. The CV of 0.01 M Na_2TeO_3 + 0.1 M tartaric acid was shown in Figure 1c. Two reduction waves, labeled A and B, respectively, were observed. As we all know, Na_2TeO_3 dissolves in tartaric acid to form $HTeO_2^+$.[12] So the reduction wave A corresponded to the reduction of $HTeO_2^+$ to Te^0, and the reduction wave B corresponded to the reduction of Te^0 to Te^{2-}.[12] A sharp oxidation peak C was observed at about 0.61 V, which corresponds to the oxidation of Te^{2-}. Figure 1d shows the CV of a Pt electrode in a solution of 0.005 M $Pb(NO_3)_2$ + 0.01 M Na_2TeO_3 + 0.1 M tartaric acid. Two reduction waves, labeled as (1) and (2), respectively, were observed. The reduction wave (1) corresponded to the reduction of $HTeO_2^+$ to Te, and the reduction wave (2) corresponded to the reduction Pb^{2+} to Pb. The oxidation peak labeled as (3) at about –0.43 V was due to the stripping of Pb, and the oxidation peak labeled as (4) at about 0.42 V corresponded to the stripping of PbTe.

On the basis of the CV results, the possible formation routes for PbTe intermetallic compounds are proposed as follows. When the electrochemical deposition is carried out with a higher potential (≥ -0.51 V), the reductions of Pb^{2+} to Pb and $HTeO_2^+$ to Te can be simultaneously happened on the surface of cathode, and this will result in a solid-state reaction between Pb and Te and the formation of PbTe intermetallic compounds.[13,14] The overall process can be represented by eqs 13. On the other hand, when the electrodeposition is carried out with a lower potential (< -0.6 V), the electroreduction of $HTeO_2^+$ to Te^{2-} on the surface of cathode will happen,[12] and Pb^{2+} ions in deposition solution will react with Te^{2-} ions to form PbTe intermetallic compounds. This formation process can be expressed by eqs 4 and 5.

$$HTeO_2 + 3H^+ + 4e \rightarrow Te + 2H_2O \quad (1)$$

$$Pb^{2+} + 2e \rightarrow Pb \quad (2)$$

$$Pb + Te \rightarrow PbTe \quad (3)$$

$$3H^+ + HTeO_2 + 6e \rightarrow Te^{2-} + 2H_2O \quad (4)$$

$$Pb^{2+} + Te^{2-} \rightarrow PbTe \quad (5)$$

Electrodeposition of PbTe thin films was carried out in solution of 0.005 M $Pb(NO_3)_2$ + 0.01 M Na_2TeO_3 + 0.10 M tartaric acid with a current density of 3.3 mA/cm^2 for 30 min, and SEM images of the deposited PbTe thin films with different magnifications are shown in images a and b in Figure 2. It can be clearly seen that the symmetrical PbTe dendritic structures have been successfully synthesized. The central trunk is consisted of orderly and regular starlike particles as shown in Figure 2b. The sizes of these starlike particles are about 400−650 nm. All the secondary branches consist of regular trigonal particles, and the sizes of these particles are about 100−250 nm. The central trunk and all the secondary branches in PbTe deposits are regularly angled, and all the angles are about 66°. All the secondary branches in these dendritic structures are almost parallel to each other. The tertiary branches are also found in the second dendritic structures. With deposition time increasing, the stem becomes longer, and new branches are formed near the tip region continuously. These new branches are shorter because of the shorter growth time. The total length of the prepared PbTe dendrites can be 10−50 μm, as shown in Figure 2a. The TEM image of PbTe dendrite is shown in Figure 3a. The typical HRTEM image and SAED pattern recorded from trunk are shown in Figure 3b, and they both demonstrated the trunk was single crystalline. The fringe spacing is determined to be 0.23 nm, which is close to the (220) lattice spacing of the rock salt PbTe, indicating that the

(12) Xiao, F.; Yoo, B.; Ryan, M. A.; Lee, K.-H.; Myung, N. V. *Electrochim. Acta* **2006**, *52*, 1101–1107.
(13) Ivanova, Y. A.; Ivanou, D. K.; Streltsov, E. A. *Electrochem. Commun.* **2007**, *9*, 599–604.
(14) Saloniemi, H.; Kanniainen, T.; Ritala, M.; Leskela, M. *Thin Solid Films* **1998**, *326*, 78–82.

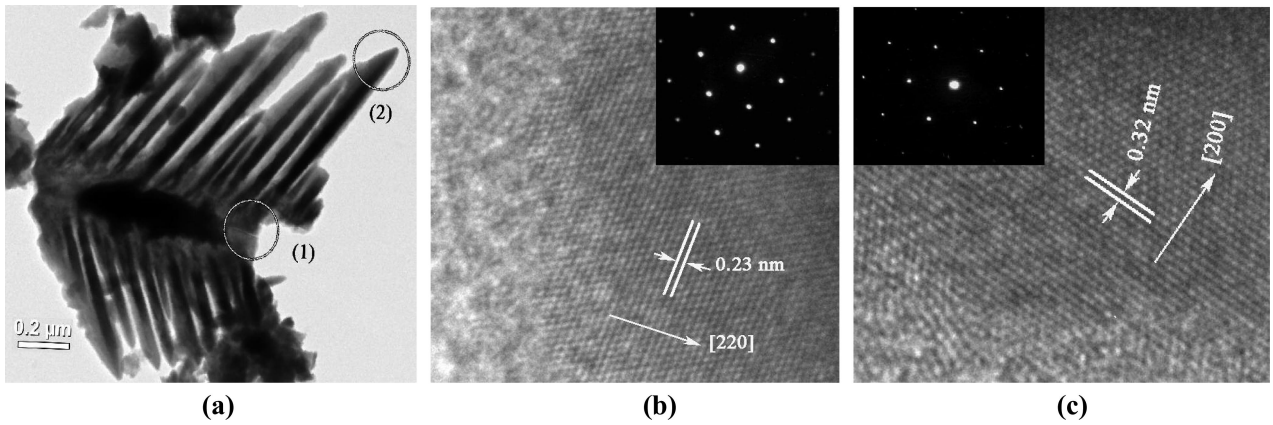

Figure 3. (a) TEM image of PbTe dendrite; (b) HRTEM image and SAED pattern of trunk of PbTe dendrite; (c) HRTEM image and SAED pattern of branch of PbTe dendrite.

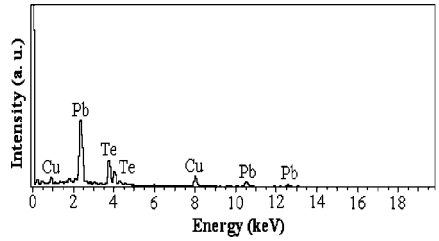

Figure 4. EDS pattern of PbTe dendritic structures. (Cu peaks correspond to the substrate).

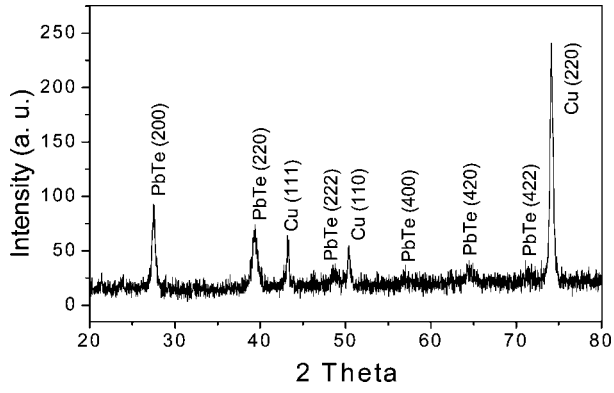

Figure 5. XRD pattern of PbTe dendritic structures. (Cu peaks correspond to the substrate).

crystal growth of the trunk is preferential in the (220) direction. The typical HRTEM image and SAED pattern recorded from branch are shown in Figure 3c. The branch in PbTe dendritic structures is also single crystalline. The fringe spacing shown in Figure 3c is determined to be 0.32 nm, which is close to the (200) lattice spacing of rock salt PbTe, indicating that the crystal growth of the branch is preferential in the (200) direction.

The representative EDS pattern of PbTe dendritic structures was shown in Figure 4. Te peaks at about 3.75 and 4.0 keV and Pb signals at about 2.41, 10.60, and 12.73 keV are observed. The composition analysis results show the PbTe intermetallic compounds were successfully electrodeposited. The Cu peaks correspond to the substrate. Further characterization by X-ray powder diffraction was carried out, and Figure 5 shows a typical XRD pattern of the PbTe dendritic structures. According to the reflection peak positions and relative intensities, the pattern can be easily indexed to PbTe. It is also clearly shown that there is no other crystalline phase besides PbTe. The lattice constant obtained by refinement of the XRD data is $a = 6.459$ Å, which is consistent with the standard valve ($a = 6.454$ Å) of bulk rock salt PbTe (JCPDS 38–1435). The prepared PbTe dendritic structures were further characterized by using X-ray photoelectron spectroscopy (XPS, ESCALAB 250), and Figure 6 shows the XPS spectra of the PbTe deposits. The Pb $4f_{7/2}$ peak at about 138 eV and $4f_{5/2}$ peak at about 143 eV are observed in Figure 6b, which proves the existence of Pb^{2+}.[15] The Te $3d_{3/2}$ and $3d_{5/2}$ peaks at about 586.2 and 575.7 eV are also observed in Figure 6c, which proves the existence of Te^{2-}.[16] The results of XPS spectra further demonstrated PbTe intermetallic compounds were successfully obtained. In addition, the small shoulders in the Pb4f and the smaller set of peaks for the Te3d spectra were observed. The survey scan of XPS analysis for the PbTe deposit was measured and it was shown in Figure 6a. The O 1s peak was observed in the survey scan, and the high-resolution scan of the O 1s peak in the XPS spectrum was shown in Figure 6d, and it proved the O element existed in the deposits. Therefore, the small shoulders in the Pb4f and the smaller set of peaks for the Te3d spectra are related to different oxidation states as the result of oxides. The formation of the oxides may be explained as follows. During electrodeposition, the Pb^{2+} ions can be electroreduced to Pb, and the $HTeO_2^+$ ions can be electroreduced to Te. As the just electroreduced Pb atoms and Te atoms are very active, part of them may react with the oxygen in deposition solution to form the oxides of Pb and Te. In addition, the surface of the PbTe crystals also can be partially oxidized because of exposure to air.[17]

The electrodeposition of PbTe was carried out in the absence of tartaric acid with and without the presence of HNO_3, and the SEM images of deposits are shown in images a and b in Figure 7, respectively. The perfect dendritic structures of PbTe were not obtained. This clearly shows the role of tartaric acid in controlling the dendritic structures of PbTe is crucial. The effect of tartaric acid in controlling

(15) Zhao, W.; Ge, P.-Y.; Xu, J.-J.; Chen, H.-Y. *Langmuir* **2007**, *23*, 8597–8601.
(16) Menke, E. J.; Brown, M. A.; Li, Q.; Hemminger, J. C.; Penner, R. M. *Langmuir* **2006**, *22*, 10564–10574.
(17) Zhu, J.-P.; Yu, S.-H.; He, Z.-B.; Jiang, J.; Chen, K.; Zhou, X.-Y. *Chem. Commun.* **2005**, 5802–5804.

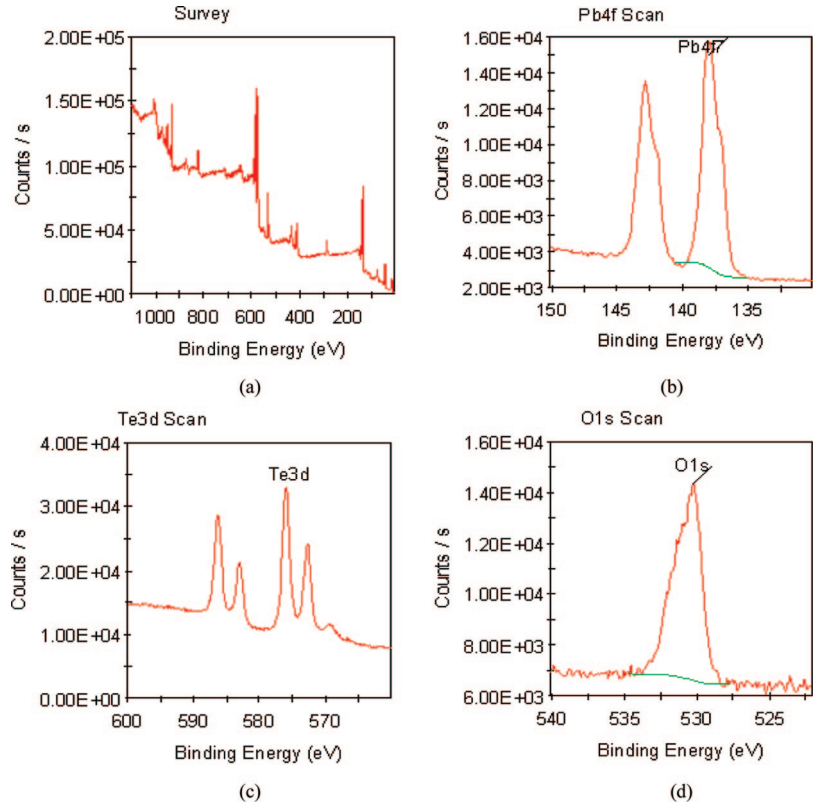

Figure 6. XPS spectra of PbTe deposits: (a) survey scan; (b) Pb 4f; (c) Te 3d; and (d) O 1s regions for PbTe dendritic structures.

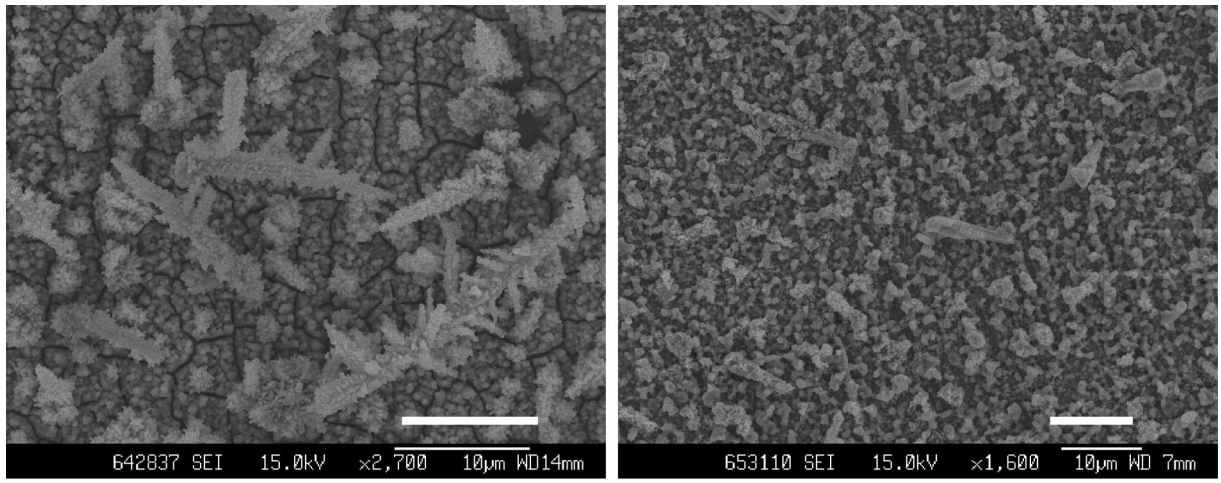

Figure 7. SEM images of PbTe deposits prepared in a solution of (a) 0.005 mol/L $Pb(NO_3)_3$ + 0.01 mol/L Na_2TeO_3 + 0.10 mol/L HNO_3; (b) 0.005 mol/L $Pb(NO_3)_3$ + 0.01 mol/L Na_2TeO_3 with a current density of 3.33 mA/cm^2 for 30 min (scan bar is 10 μm).

the surface morphology can be attributed to following reasons: (1) The complexes can be formed between Pb^{2+} and tartaric acid, and the concentration of free Pb^{2+} ions will be decreased. Accordingly, the deposition rate of PbTe will be decreased, and this will affect the surface morphology. (2) The effect of tartaric acid on the growth of PbTe dendritic structures possibly can be attributed to specific interactions between PbTe nuclei and tartaric acid. In the synthesis of materials, it is well-known that some capping molecules can block the crystal growth of certain directions and enhance the crystal growth of other directions.[18] Here, we also believe that the capping effect of tartaric acid plays a key role for the growth of PbTe dendritic structures. In addition, we also investigated the different time intervals for a better understanding of the growth, and the SEM images are shown in Figure 8. When the deposition time was 60 min, the density of dendritic structures was much higher than that of dendritic structures prepared for 10 min.

When the current density of electrodeposition was decreased from 3.3 to 1.0 mA/cm^2 for 60 min, the perfect dendrites were also successfully obtained as shown in Figure 9. It should be noted that the prepared dendrites were

(18) (a) Epifani, M.; Arbiol, J.; Diaz, R.; Peralvarez, M. J.; Siciliano, P.; Morante, J. R. *Chem. Mater.* **2005**, *17*, 6468–6472. (b) Shevchenko, E. V.; Talapin, D. V.; Rogach, A. L.; Kornowski, A.; Haase, M.; Weller, H. *J. Am. Chem. Soc.* **2002**, *124*, 11480–11485.

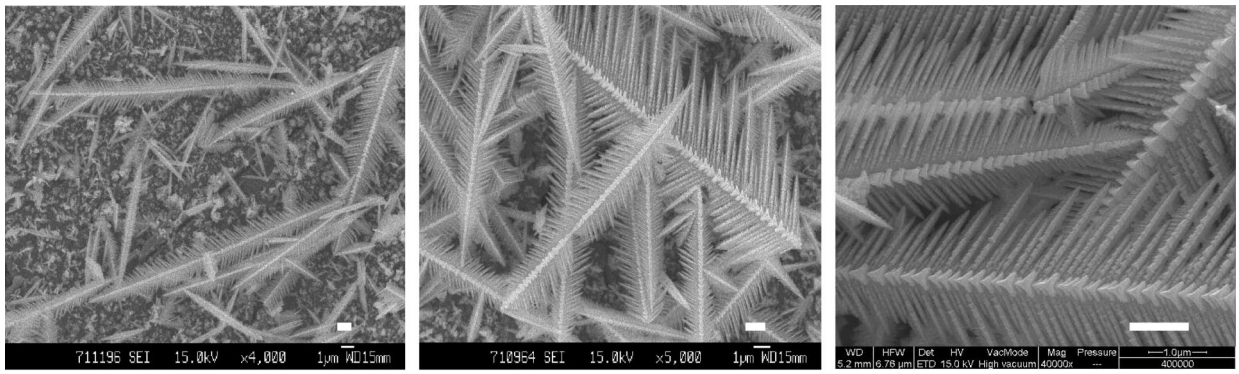

Figure 8. Comparison between SEM images of PbTe dendritic structures prepared for (a) 10, (b) 30, and (b) 60 min in a solution of 0.005 mol/L $Pb(NO_3)_3$ + 0.01 mol/L Na_2TeO_3 + 0.10 mol/L tartaric acid with a current density of 3.33 mA/cm^2 (scan bar is 1 μm).

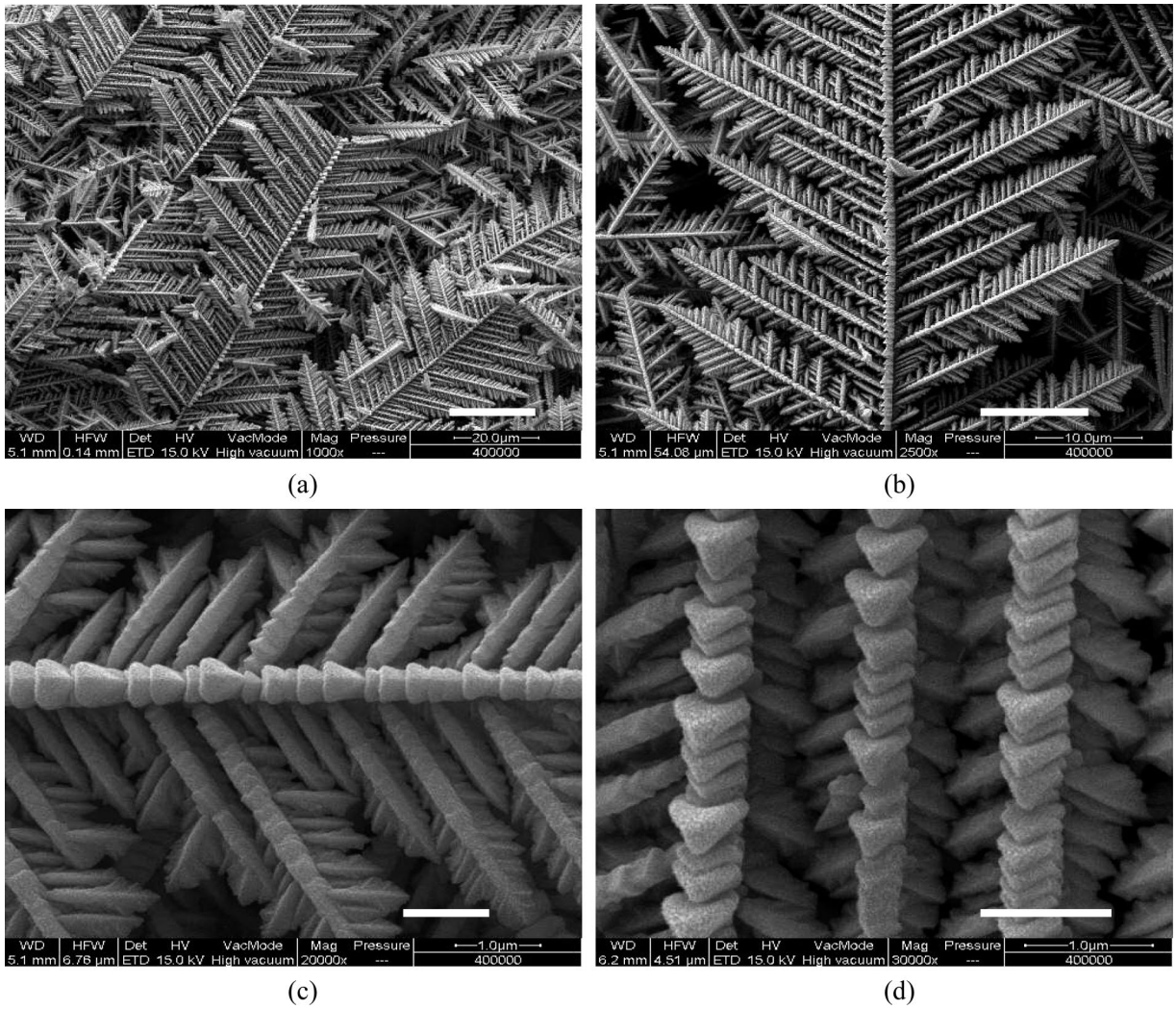

Figure 9. SEM images of PbTe dendritic structures prepared in a solution of 0.005 M $Pb(NO_3)_2$ + 0.01 M Na_2TeO_3 + 0.10 M tartaric acid for 60 min with a current density of 1.0 mA/cm^2. (a) Panorama of PbTe deposit (scan bar is 20 μm); (b) single dendrite (scan bar is 10 μm); (c) secondary branch (scan bar is 1 μm); (d) tertiary branches (scan bar is 1 μm).

different from those shown in Figure 2. Although the central trunks in Figure 9a also consist of particles, the shapes of these particles obviously changed. The central trunk consists of orderly and regular trigonal particles as shown in Figure 9b. The average sizes of these particles are about 700 nm. The secondary, tertiary, and quartus branches are also observed in these dendritic structures as shown in Figure 9b−d, respectively. It is interesting that the angles formed by the central trunk and the secondary branches are regular, and all of them are about 62°. Therefore, all the secondary branches in the above dendritic structures are almost parallel to each other. Furthermore, all the secondary and tertiary branches in the prepared PbTe dendritic structures also consist of uniform and regular trigonal particles as shown

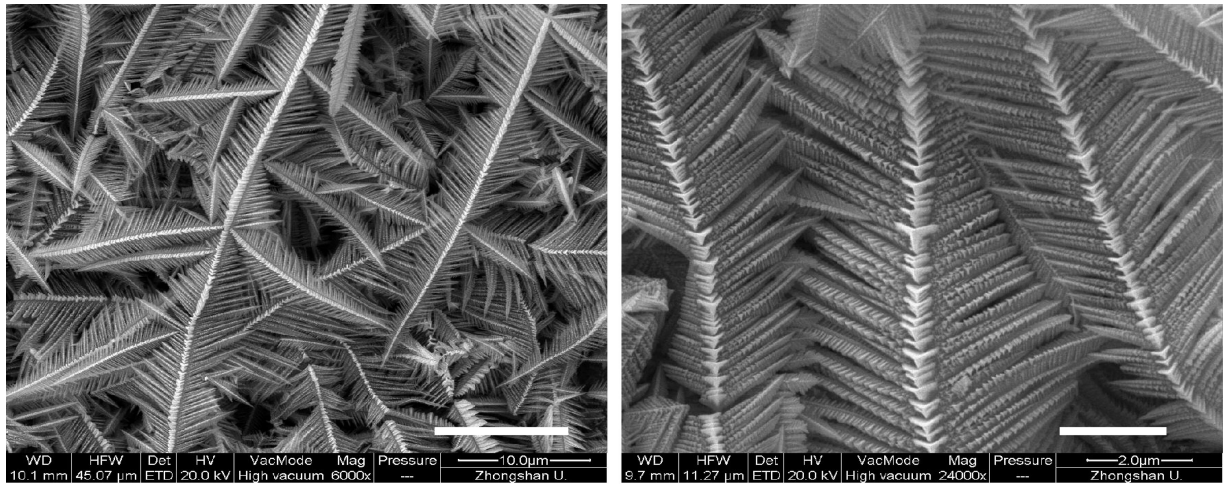

Figure 10. SEM images of PbTe dendritic structures prepared in a solution of 0.005 M $Pb(NO_3)_2$ + 0.01 M Na_2TeO_3 + 0.10 M tartaric acid for 30 min with a current density of 3.33 mA/cm^2. (a) Ni substrate (scan bar is 10 μm); (b) Ti substrate (scan bar is 2 μm).

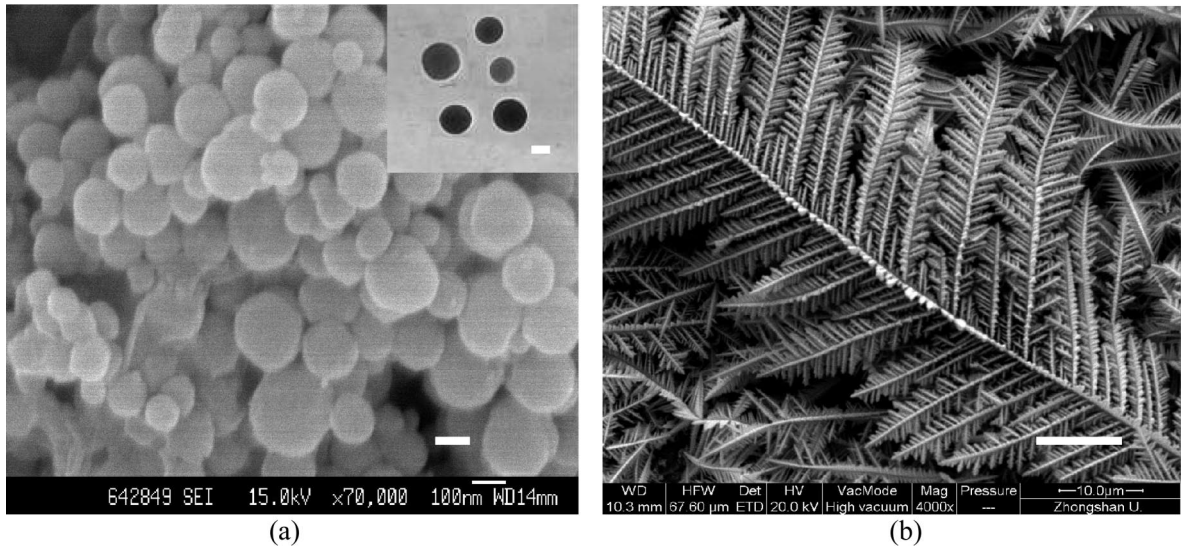

Figure 11. (a) SEM image of PbTe dendritic structures prepared in a solution of 0.01 mol/L $Pb(NO_3)_3$ + 0.005 mol/L Na_2TeO_3 + 0.10 mol/L tartaric acid at 0.02 mA/cm^2 (near equilibrium) and TEM image (inset) (scan bar is 100 nm); (b) SEM image of PbTe dendritic structures prepared in a solution of 0.01 mol/L $Pb(NO_3)_3$ + 0.005 mol/L Na_2TeO_3 + 0.10 mol/L tartaric acid at 3.33 mA/cm^2 (far away from equilibrium) for 30 min (scan bar is 10 μm).

in images c and d in Figure 9, respectively. The sizes of the trigonal particles in the second branches are smaller than those in the central trunk, which may be caused by the shorter deposition time. Also, the trigonal particles in the tertiary branches are smaller than those in the secondary branches, and they are about 200−300 nm. These tertiary branches are also almost parallel to each other as shown in images c and d in Figure 9. However, the leaflike particles are observed in the quartus branches as shown in Figure 9d. The effects of various substrates on the surface morphologies of PbTe deposits were also investigated. When the electrodeposition was carried out on Ni or Ti substrates in a solution of 0.005 M $Pb(NO_3)_2$ + 0.01 M Na_2TeO_3 + 0.10 M tartaric acid with a current density of 3.3 mA/cm^2 for 30 min, the similar PbTe dendritic structures were also obtained as shown in Figure 10.

The surface morphologies of crystals depend on the deviation degree of the formation conditions from the thermodynamic equilibrium or the driving force for crystallization.[19] The polyhedral crystals with thermodynamically stable crystal faces and a minimum surface energy will form when the surrounding condition is near-equilibrium condition. However, the dendrites will form when the formation conditions are far from the thermodynamic equilibrium because of the increasing of the contribution of mass diffusion.[20] The comparison between near-equilibrium growth and growth far from equilibrium has been made to show the change in morphology of the deposited films, and the SEM images of deposits were shown Figure 11. In other words, when the crystal growth rate is lager than that of the mass transport of ions that feed the growing crystals, the dendritic growth will be promoted. The form conditions of deposits during electrodeposition can be near or far equilibrium state

(19) (a) Kuroda, T.; Irisawa, T.; Ookawa, A. *J. Cryst. Growth* **1977**, *42*, 41–46. (b) Oaki, Y.; Imai, H. *Cryst. Growth Des.* **2003**, *3*, 711–716.
(20) Fukami, K.; Nakanishi, S.; Yamasaki, H.; Tada, T.; Sonoda, K.; Kamikawa, N.; Tsuji, N.; Sakaguchi, H.; Nakato, Y. *J. Phys. Chem. C* **2007**, *111*, 1150–1160.

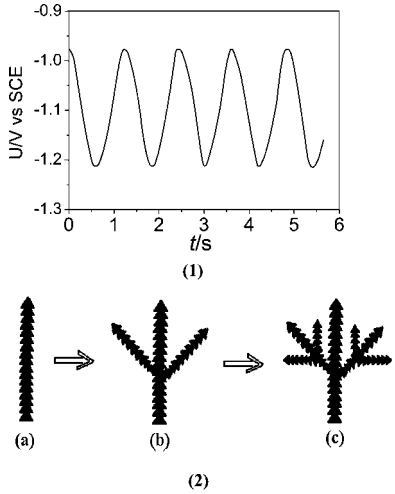

Figure 12. (1) Potential oscillations under the galvanostatic conditions (3.3 mA/cm^2); (2) simple schematic description of the growth process of PbTe dendritic structures.

by tuning continuously and reversibly by simply changing the deposition potential or current density,[19] namely, the interplay between the crystal growth rate and the mass transport rate can be altered without changing reactant concentrations. In this experiment, the electrodeposition of PbTe was carried out with a current density of 1.0−3.3 mA/cm^2, and the current density is much higher than the diffusion-limited one. So the electrodeposition condition of PbTe is far from the thermodynamic equilibrium. During the electrodeposition under galvanostatic conditions, the electrode potential oscillations can be often observed when the current is sufficiently high and exceeds the diffusion-limited one.[19] Figure 12(1) shows the electrode potential oscillations under the galvanostatic condition with current density of 3.3 mA/cm^2. Therefore, the formation of the PbTe dendrites with ordered periodic structures can be successfully realized when the dendrite growth proceeds in synchronization with the potential oscillations. On the basis of the experimental results, the sizes of particles are gradually decreased from trunk to branches and subbranches. The particle size is obviously correlative to the growth time. Therefore, the formation process of PbTe dendritic structures comply following rules: first, the PbTe particles chain as the trunk is formed, and the crystal growth is along [220] direction according to the results of TEM and SAED shown in Figure 3. Subsequently, the secondary branches branch off along [200] direction. With further growth, the tertiary families of branches grow out from the secondary branches. The whole growth process of PbTe dendritic structures during electrodeposition was simply described in Figure 12(2).

The detailed process for the formation of seasonal PbTe particles in dendritic structures is clarified as follows. During the electrodeposition, Pb^{2+} and $HTeO_2^+$ ions in solution will be driven to the cathode under the electric field, and are then electroreduced. PbTe particles will be released in sites arbitrarily on the Cu substrate and will then be irreversibly stuck to each other to grow the clusters. It is well-known that the pH in deposition solution has something to do with

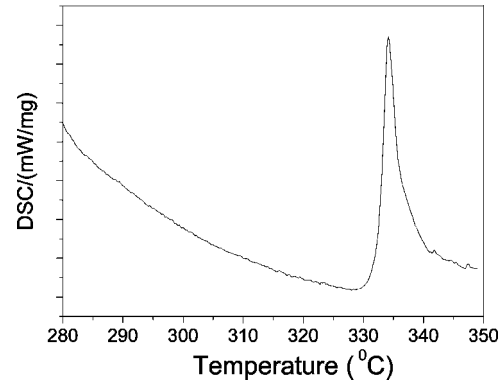

Figure 13. DSC curve of PbTe dendritic structures prepared in a 0.005 M $Pb(NO_3)_2$ + 0.01 M Na_2TeO_3 + 0.10 M tartaric acid solution.

it.[21] Tartrate is present to act as a buffer. As the potential decreases, so that the assigned current density is maintained, more water decomposition or hydrogen evolution would result. The pH of the deposition solution, which can affect the existence of $HTeO_2^+$, will increase, and the deposition rate of PbTe will become slow according to eq 1. Therefore, more ions will be allowed to diffuse back into the film, and fewer protons will then be reduced. Subsequently, the pH in deposition solution will decrease, and the deposition of PbTe will increase again. The new deposited PbTe particles may stick to any parts of the formed clusters but are more likely to encounter the tips of the clusters than to penetrate deep into its inner regions, leading to outward growth from the initial location of seed particles.[22] Therefore, with electrodeposition time increasing, the dendritic structures consisted of orderly and regular trigonal particles.

DSC analyses were conducted to study the thermal properties of the prepared PbTe dendritic structures. An exothermic peak at about 334 °C was observed in the DSC curve shown in Figure 13. This peak will disappear when the sample is cooled to room temperature and reheated in the same temperature range. The presence of such an exothermic transition may be result of the internal strain energy in the as-deposited PbTe dendritic structures.[23] However, the temperature of exothermic peak of PbTe dendritic structures is much higher than that of other PbTe reported in the literature,[20] which shows the strain in the as-deposited PbTe dendritic structures is smaller. According to the PbTe compounds prepared by sonochemcial and microwave route, two endothermic peaks at about 408 and 440 °C related to the eutectic transition between PbTe and Te and to the transition PbTe + L → PbTe, respectively, were observed in DSC curve, which shows the coexistence of PbTe and Te in the prepared compounds.[22] However, in our experiment, no endothermic peak was observed in DSC analysis before the melting point of PbTe, about 924 °C, which shows that the prepared deposits are highly pure PbTe. These results are in very good agreement with the results of EDS, XRD, and XPS.

(21) Li, G. R.; Lu, X.-H; Qu, D.-L; Yao, C.-Z; Zheng, F.-L; Bu, Q.; Dawa, C.-R.; TongY.-X, *J. Phys. Chem. C* **2007**, *111*, 6678–6683.
(22) Ng, C. H. B.; Tan, H.; Fan, W. Y. *Langmuir* **2006**, *22*, 9712–9717.
(23) Kerner, R.; Palchik, O.; Gedanken, A. *Chem. Mater.* **2001**, *13*, 1413–1419.

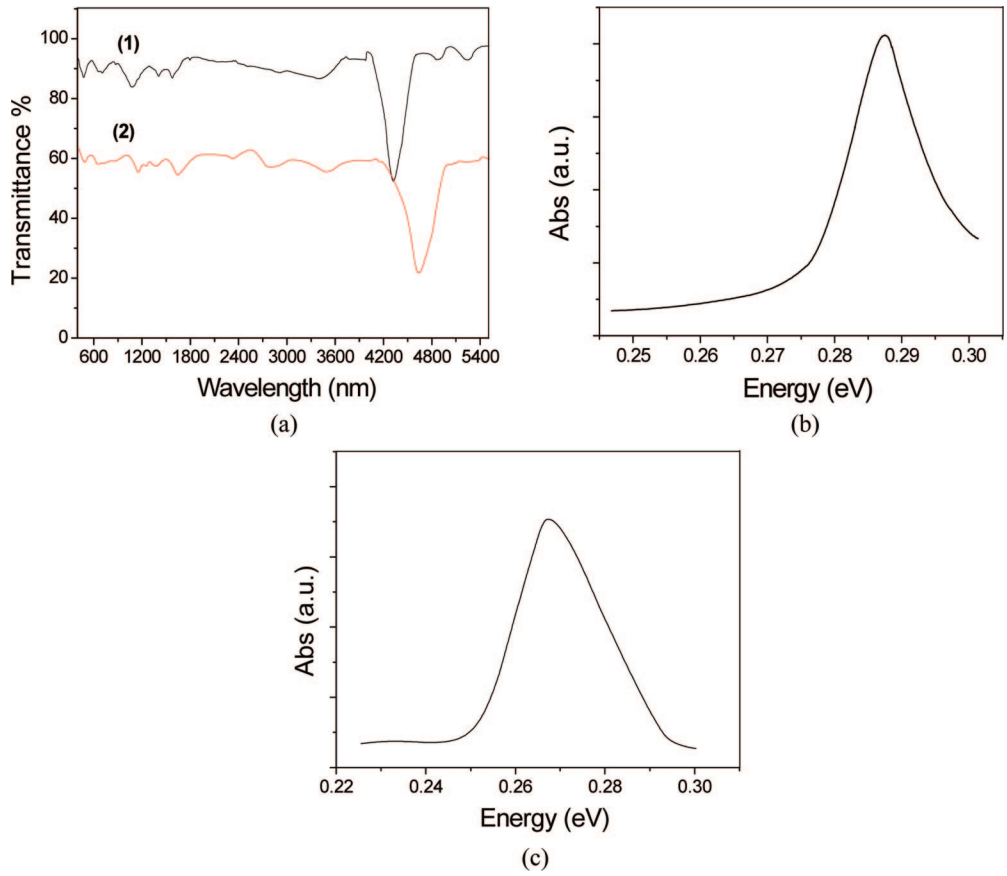

Figure 14. (a) IR spectra of PbTe dendritic structures (1) and PbTe nanoparticles (2); (b) IR absorption spectrum of PbTe dendritic structures; (c) IR absorption spectrum of PbTe nanoparticles.

The optical property of deposited PbTe dendritic structures was investigated with FT-IR spectrometer. The IR spectra in 400−5000 nm region for PbTe dendritic structures deposited with 3.33 mA/cm^2 and PbTe particles deposited with 0.02 mA/cm^2 are shown in Figure 14a (1) and Figure 14a (2), respectively. It can be obviously seen that the optical response of the prepared PbTe dendritic structures shows high transmittance (about 90%) at low frequencies (400−4000 nm), which is much higher than that of PbTe nanoparticles. Compared with PbTe colloidal nanocrystals,[24] the strong effect of dendritic structures on the optical property also can be obviously observed. The absorption spectrum between 0.245−0.300 eV for PbTe dendritic structures was shown in Figure 14b. A sharp absorption peak was observed at near 0.284 eV. According to the data for the absorption spectra, the optical band gaps (E_g) of PbTe can be estimated by using the following equation.

$$\alpha h\nu = C(h\nu - E_g)^n$$

Here, α is the absorption coefficient, $h\nu$ is photon energy, and C is a constant. The band gap energy of the prepared PbTe dendritic structures was calculated about 0.272 eV, which is bigger than that of PbTe nanoparticles obtained form Figure 14c and the literature value.[25]

3. Conclusions

In summary, we reported here a facile and efficient synthesis route for the preparation of PbTe dendritic structures consisting of orderly and regular particles via electrochemical deposition without any templates. The electrode potential oscillation is relevant to the formation of the PbTe dendrites. The sizes of the particles are tunable from 100 to 500 nm and the shapes can be controlled to be either starlike or trigonal. The high transmittance of the PbTe dendritic structures in the 500−4000 nm region is observed, and the band gap energy of the prepared PbTe dendrites can be calculated to be about 0.272 eV. The unique synthetic mechanism of this approach is expected to generate other intermetallic compound dendrites of technological importance with well-controlled architectures.

Acknowledgment. We appreciated the support of this work by the Natural Science Foundations of China (Grants 20603048 and 20573136), the Natural Science Foundations of Guangdong Province (Grants 06300070, 06023099, and 04205405), and the Foundations of Potentially Important Natural Science Research and Young Teacher Starting-up Research of Sun Yat-Sen University.

CM8001942

(24) Murphy, J. E.; Beard, M. C.; Norman, A. G.; Ahrenkiel, S. P.; Johnson, J. C.; Yu, P.; Mićić, O. I.; Ellingson, R. J.; Nozik, A. J. *J. Am. Chem. Soc.* **2006**, *128*, 3241–3247.

(25) Mondal, A.; Mukherjee, N.; Kumar Bhar, S.; Banerjee, D. *Thin Solid Films* **2006**, *515*, 1255–1259.